Microbial Cell Factories

RESEARCH

Open Access

Engineering of global transcription factor FruR to redirect the carbon flow in *Escherichia coli* for enhancing L-phenylalanine biosynthesis

Minliang Chen[1,3*], Hengyu Liang[1,2,3*], Chao Han[1,3], Peng Zhou[1,3], Zhiwei Xing[1,2], Qianqian Chen[3], Yongyu Liu[1], Gou-an Xie[1] and Rufei Xie[1]

Abstract

Background: The catabolite repressor/activator protein (FruR) is a global regulatory protein known to control the expression of several genes concerned with carbon utilization and energy metabolism. This study aimed to illustrate effects of the FruR mutant on the L-phenylalanine (L-PHE) producing strain PHE01.

Results: Random mutagenesis libraries of *fruR* generated in vitro were first integrated into the chromosome of PHE01 by CRISPR/Cas9 technique, and then the best mutant PHE07 ($FruR^{E173K}$) was obtained. With this mutant, a final L-PHE concentration of 70.50 ± 1.02 g/L was achieved, which was 23.34% higher than that of PHE01. To better understand the mechanism, both transcriptomes and metabolomes of PHE07 were carried out and compared to that of PHE01. Specifically, the transcript levels of genes involved in gluconeogenesis pathway, pentose phosphate pathway, Krebs cycle, and glyoxylate shunt were up-regulated in the $FruR^{E173K}$ mutant, whereas genes *aceEF, acnB*, and *icd* were down-regulated. From the metabolite level, the $FruR^{E173K}$ mutation led to an accumulation of pentose phosphate pathway and Krebs cycle products, whereas the products of pyruvate metabolism pathway: acetyl-CoA and *cis*-aconic acid, were down-regulated. As a result of the altered metabolic flows, the utilization of carbon sources was improved and the supply of precursors (phosphoenolpyruvate and erythrose 4-phosphate) for L-PHE biosynthesis was increased, which together led to the enhanced production of L-PHE.

Conclusion: A novel strategy for L-PHE overproduction by modification of the global transcription factor FruR in *E. coli* was reported. Especially, these findings expand the scope of pathways affected by the *fruR* regulon and illustrate its importance as a global regulator in L-PHE production.

Keywords: FruR, L-phenylalanine, Transcriptome, Metabolome, CRISPR/Cas9

Background

L-phenylalanine (L-PHE), which is an essential amino acid, has wide applications in food, agricultural, and pharmaceutical industries, and it is also an important chiral substrate for the synthesis of the low-calorie sweetener aspartame (L-phenylalanyl-L-aspartyl-methyl ester) [1, 2]. In recent years, as one of the aromatic amino acids, L-PHE production via metabolically engineered microbes, e.g., *Corynebacterium glutamicum* [3] and *Escherichia coli* [4, 5], has become more promising than other production routes, e.g., chemical synthesis or hydrolytic cleavage of proteins.

In *E. coli*, the biosynthetic pathway of L-PHE can be divided into two parts: the chorismate pathway and the L-PHE branch. The chorismate pathway connects the glycolysis and the pentose phosphate pathway and ends in

*Correspondence: Minliang202208@163.com; lhy-410@163.com

[1] Henan Joincare Biopharma Research Institute Co. Ltd, Jinyuan Street 8, Jiaozuo 454000, People's Republic of China
Full list of author information is available at the end of the article

the formation of chorismate. It begins with the condensation of the phosphoenolpyruvate (PEP) and erythrose 4-phosphate (E4P) to form 3-deoxy-D-arabinoheptulosonate-7-phosphate (DAHP). In the $_{L}$-PHE branch, $_{L}$-PHE is produced from chorismate in two steps catalyzed by the enzymes encoded by *pheA* and *tyrB* [6]. Till now, considerable attention has been paid to the sustainable production of $_{L}$-PHE in microbial cells using the strategies of rational metabolic engineering, including (i) alleviation of all restrictive regulations [7–9]; (ii) deletion of competing pathways [5]; (iii) enhancement and balancing of precursor supplements [10, 11]; and (iv) removal of $_{L}$-PHE degradation pathway. However, current strategies are mainly focused on the engineering of $_{L}$-PHE biosynthetic pathway itself, and it is challenging to generate a high production of the desired chemical by these classical engineering approaches [5]. In recent years, transcriptional engineering approaches have been applied to strain optimization, which makes the engineering process carried out at a global and systematic level [12–14]. The global regulation of metabolic networks through multiple transcription factors (TFs) is one of the complex mechanisms for prokaryotes to respond to the intracellular perturbations by altering the expression of related genes [15, 16]. As an important component of gene expression regulation, modification of TFs can cause changes in carbon flux in the relevant metabolic pathways; thus, engineering of TFs has been proved to be useful for redirecting the fluxes toward the desired pathway for improving the target component [17–19]. However, to the best of our knowledge, few work has been reported to improve the $_{L}$-PHE biosynthesis by TFs engineering.

FruR (catabolite repressor/activator, also known as Cra), is known to regulate the expression of several genes concerned with carbon utilization and energy metabolism [20–22]. FruR is a dual transcriptional regulator and it modulates the direction of carbon flow by transcriptional activation of genes encoding enzymes concerned with the Krebs cycle and the glyoxylate shunt and by repression of those genes that are involved in the glycolytic and Entner-Doudoroff (ED) pathways [23, 24]. In a previous study, the influence of *fruR* knockout on tryptophan biosynthesis was reported [17], and the metabolomics analysis showed that *fruR* knockout significantly enhanced the metabolic flow toward glycolysis, pentose phosphate pathway, and TCA cycle, increasing levels of critical precursors and substrates for $_{L}$-tryptophan biosynthesis. A similar result was also reported by Zeng group [9]. However, to our surprise, it was found that inactivating the global regulator FruR in our $_{L}$-PHE-producing strain PHE01 led to a significant decrease in $_{L}$-PHE production. This result revealed that the regulation effects of FruR are more complex than expected and it is worth exploring the mechanism further.

Table 1 $_{L}$-PHE fermentation parameters of the strains PHE01 and PHE03

Strain	OD610	$_{L}$-PHE (g/L)	Vp (g/L/h)	q_{PHE} (mg PHE/g DCW/h)
PHE01	39.05 ± 0.56	7.02 ± 0.23	0.16 ± 0.05	11.95 ± 1.03
PHE03	36.50 ± 0.05	5.75 ± 0.55	0.13 ± 0.02	10.46 ± 0.81

The engineered $_{L}$-PHE-producing strains were cultivated in 500 mL shake flasks for 43 h

The data represents the mean ± SD from three independent experiments

Vp volumetric productivity, q_{PHE} specific production rate of $_{L}$-PHE

In this study, the functionality of the global regulator FruR for $_{L}$-PHE over production was first verified. Then, CRISPR/Cas9-facilitated engineering was combined with sensor-guided in vivo screening for engineering of protein FruR. In order to clarify the regulation mechanism of FruR, comparison of multi-omics data was performed between the best mutant and the wild-type strains.

Results and discussion

Knockout of *fruR* affects the biosynthesis of $_{L}$-PHE

To explore the impact of FruR on the biosynthesis of $_{L}$-PHE, the gene *fruR* in our previously constructed $_{L}$-PHE-producing strain PHE01/pCas9 was disrupted, generating the strain PHE03 (Table 4, details in Additional files 3). The capacity of $_{L}$-PHE production of PHE03 was compared to that of strain PHE01 by carrying out shake-flask fermentations (Table 1).

Table 1 shows that the cultivation of both strains PHE01 and PHE03 obtained almost the same amount of biomass. However, at the end of fermentation, PHE03 produced 5.75 ± 0.55 g/L of $_{L}$-PHE, which is 18.10% lower than that of the strain PHE01 (7.02 ± 0.23 g/L). Meanwhile, the productivity (Vp) and specific production rate (q_{PHE}) were also significantly decreased. These results suggested that the disruption of regulator FruR could result in the imbalance of central carbon metabolism, and indirectly block the metabolic flow toward the $_{L}$-PHE biosynthetic pathway. Also, this result demonstrated that the regulation functionality of protein FruR is critical for $_{L}$-PHE overproduction, and this was not consistent with the reported case for L-tryptophan [9, 17]. To find out whether modification of the regulation functionality of protein FruR could increase the production of $_{L}$-PHE, a random mutagenesis strategy combined with the $_{L}$-PHE biosensor was employed for the engineering and characterization of FruR mutants.

Engineering and characterization of FruR mutants

To obtain a FruR mutant with a higher production of $_{L}$-PHE, the *fruR* variants were generated in vitro by using the error-prone PCR, and then the resulting gene variants were integrated into the chromosome of PHE01/pCas9 using the CRISPR/Cas9 technique. Finally, the FruR mutants were screened and characterized with the aid of $_{L}$-PHE biosensor and HPLC detection.

Firstly, a host strain PHE01Δ*fruR*::Cm^R (Table 4, details in Additional files 3) was constructed by inserting a chloramphenicol resistance gene Cm^R into the locus of the *fruR* gene to offer the sgRNA target sequence for CRISPR/Cas9 application in further gene variant integration. In principle, an engineered FruR protein with a higher activity should lead to more accumulation of $_{L}$-PHE, which in turn stimulate the expression of a report gene regulated by an $_{L}$-PHE biosensor. The $_{L}$-PHE biosensor is composed of the promoter of *mtr* gene (p*mtr*) [25] with RFP protein fused to the downstream (Fig. 1a). In detail, the plasmid backbone, upstream of the transcriptional start site of the p*mtr* promoter, and the DNA fragment encoding for RFP protein were amplified from the plasmid pBR332, the genomic DNA of *E. coli* K-12 W3110, and the template pET28a-RFP, respectively. All fragments were then pooled to an equimolar concentration and fused together to result in the final plasmid p*mtr*-RFP (details in Additional files 3). To characterize the designed biosensor, the plasmid p*mtr*-RFP expressed with the $_{L}$-PHE biosensor was introduced into the host strain *E. coli* W3110. As observed in Fig. 1b, the $_{L}$-PHE biosensor was able to activate RFP expression by a maximum of 23.86-fold upon supplementing $_{L}$-PHE (0–200 μM) to the cultivation medium. To further validate the $_{L}$-PHE biosensor, we measured fluorescence output in five different genotypes cultivated in the M9 medium, e.g., W3110, PHE01, PHE03, PHE04 (PHE 01Δ$aroF^{MT}$::$aroF^{WT}$, details in Additional files 3), and PHE05 (PHE01Δ$pheA^{MT}$::$pheA^{WT}$, details in Additional

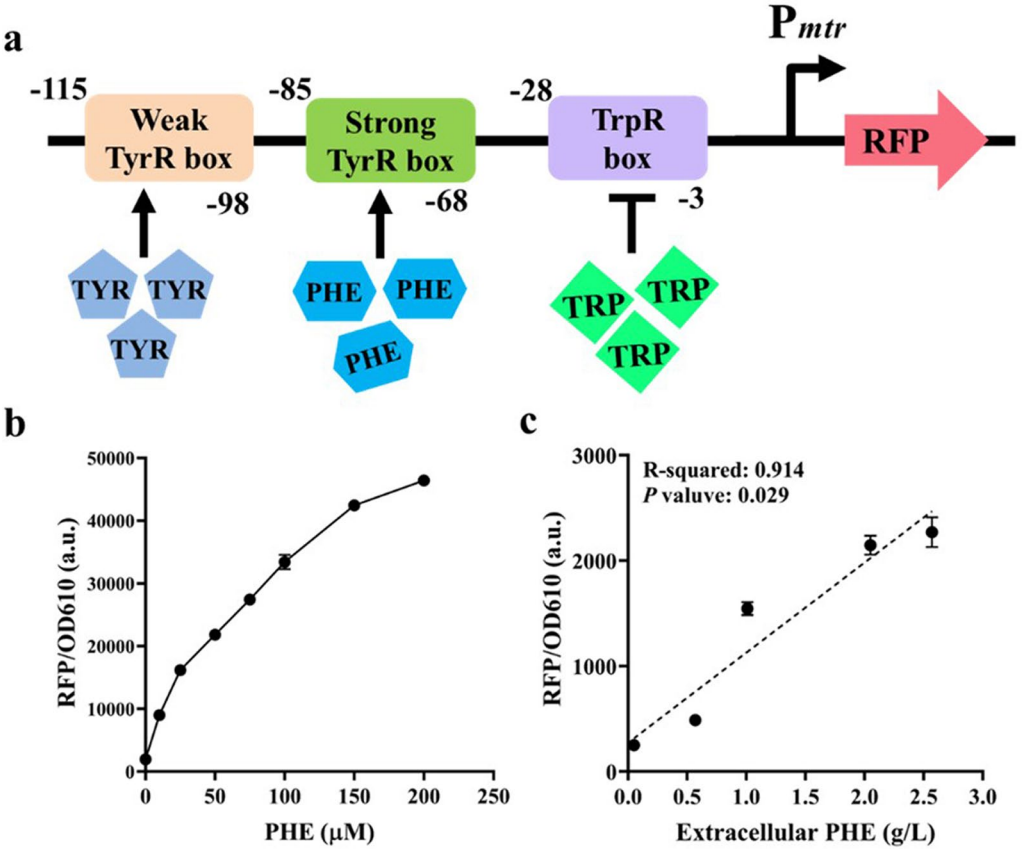

Fig. 1 Library screening and characterization using an $_{L}$-PHE biosensor. **a** Schematic illustration of the design of the $_{L}$-PHE biosensor used in this study. The $_{L}$-PHE biosensor (P*mtr*) is composed of a weak TyrR box (L-tyrosine binding site), a strong TyrR box ($_{L}$-PHE binding site), and a TrpR box (L-tryptophan binding site). The biosensor regulates the expression of an engineered reporter (RFP) and placed upstream of the RFP reporter. **b** Fluorescence normalized by OD_{610} related to concentration of $_{L}$-PHE supplemented into the media. **c** Extracellular $_{L}$-PHE normalized by OD_{610} related to fluorescence normalized by OD_{610} (mean values with standard errors, $n = 3$ technical replicates). The *p*-value showing a significant slope is from a two-side *t*-test performed on means values for the five different strains, e.g., W3110, PHE01, PHE03, PHE04, and PHE05

files 3), and observed different biosensor outputs from these strains in line with the extracellular $_{L}$-PHE concentration in strains with different genotypes ($R^2 = 0.914$ and $p = 0.029$, Fig. 1c). These results demonstrated that the designed $_{L}$-PHE biosensor has the ability to monitor changes in endogenously produced $_{L}$-PHE pools.

Having established an $_{L}$-PHE biosensor (Fig. 1), we next sought to apply the $_{L}$-PHE biosensor for high-throughput screening and characterization of the FruR variants. To do so, PHE06 was constructed by introducing the plasmid p*mtr*-RFP into PHE01Δ*fruR*::Cm^R/pCas9. Afterwards, a mutagenesis library of the *fruR* variant library was generated in vitro by using a Diversify® PCR Random Mutagenesis Kit (PT3393-2, Takara Bio) and integrated into the chromosome of host PHE06 using the CRISPR/Cas9 technique. Finally, the mutants were screened and selected by using $_{L}$-PHE biosensor-based in vivo characterization and HPLC-facilitated in vitro detection.

After the first-round screening, 279 colonies of the FruR mutants, which have relatively higher fluorescence signals, were selected and cultivated in three 96 deep-well plates. After 15 h of cultivation, cell growth and fluorescence intensity were measured and the results are presented in heat maps (Fig. 2). Among them, 50 mutants with a stronger fluorescence intensity (colored in red in Fig. 2) were isolated for sequencing. Sequencing results showed that there are 8 different types of FruR variants among these 50 candidates (Table 2), they are 40% for $FruR^{E173K}$, 22% for $FruR^{A18P}$, 16% for $FruR^{L3F-L170N}$, 10% for $FruR^{S75I-V160E}$, 6% for $FruR^{P129H}$, 2% for $FruR^{I144T}$, 2% for $FruR^{E72R-P128A}$, and 2% for $FruR^{R312G}$. Afterwards, all of these 8 types of recombinants were subjected to batch

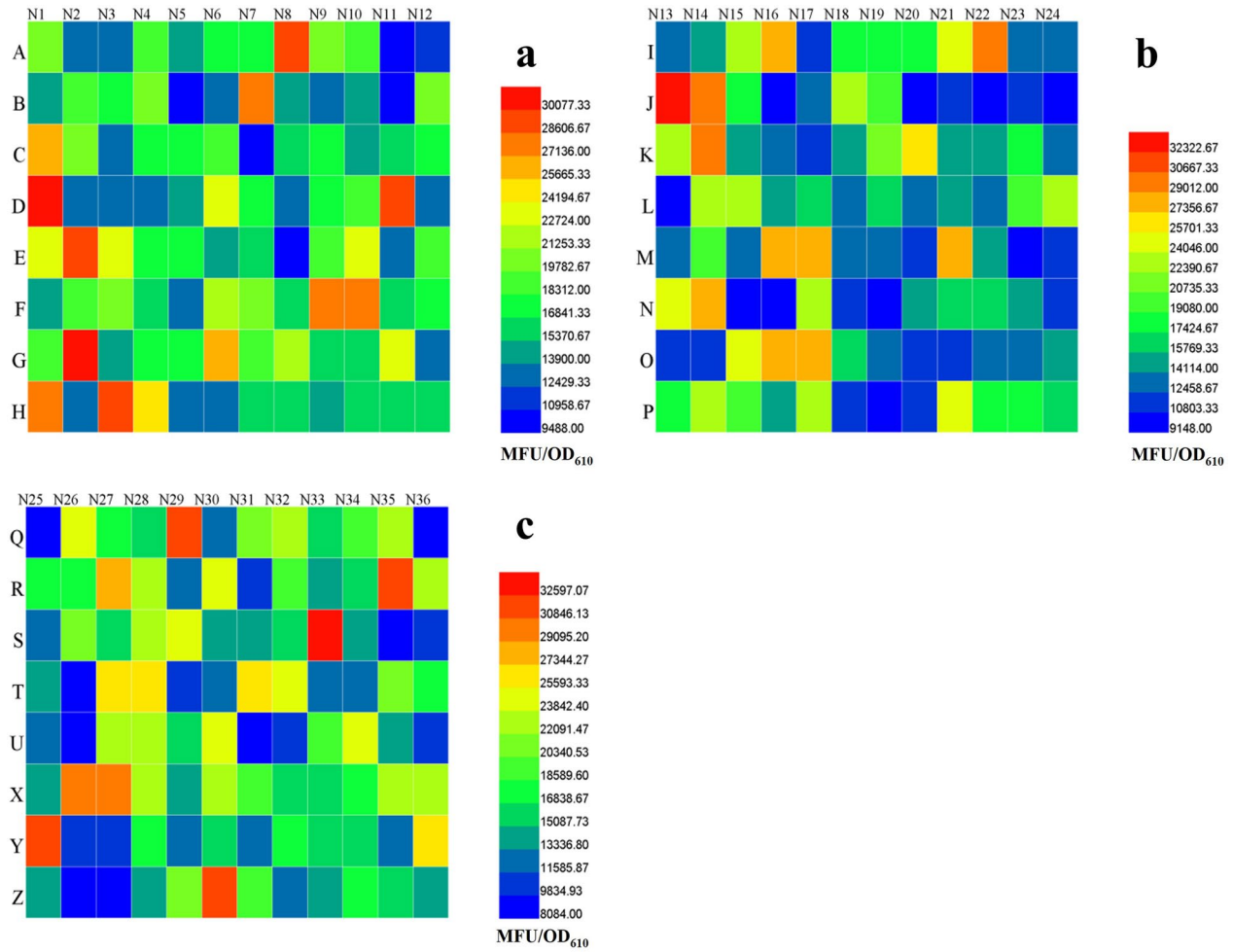

Fig. 2 Heat maps of cell growth (OD_{610}) and fluorescence intensity (MFU) of the selected mutants. A total of 276 samples in each well are presented as single colonies (**a**, **b**, and **c**). A total of 9 samples in H10-H12, P10-P12, and Z10-Z12 wells are presented as the controls: PHE01. The cells were cultured with fermentation medium in a 96-deep well plate

Table 2 Comparison of fermentation results with FruR mutants and PHE01

Mutants	Percentage [a]	OD_{610}	$_{L}$-PHE (g/L)
$FruR^{E173K}$	40	37.36 ± 0.25	9.06 ± 0.34
$FruR^{A18P}$	22	36.50 ± 0.05	8.86 ± 0.62
$FruR^{L3F-L170N}$	16	33.95 ± 1.05	7.79 ± 1.05
$FruR^{S75I-V160E}$	10	34.43 ± 1.12	8.31 ± 0.67
$FruR^{P129H}$	6	34.52 ± 2.15	8.46 ± 0.69
$FruR^{I144T}$	2	35.12 ± 1.03	8.05 ± 0.42
$FruR^{E72R-P128A}$	2	28.51 ± 1.35	7.69 ± 0.36
$FruR^{R312G}$	2	27.35 ± 0.25	7.48 ± 0.47
PHE01 [b]	–	36.06 ± 0.35	7.32 ± 0.35

[a] "Proportion" refers to the percentage of different types of mutants in all 50 candidates (%)

[b] Means the strain PHE01is used as a positive control; The fermentations were performed with a single clone for each FruR-variant

The average value ± standard deviation is based on three independent experiments

fermentation in shake flasks together with the positive control PHE01 (Table 2). As shown in Table 2, all of the selected FruR mutants had a higher $_{L}$-PHE production compared to the strain PHE01. Especially, the $FruR^{E173K}$ mutant exhibited the highest $_{L}$-PHE production among all types of mutants. These results suggest that the variant $FruR^{E173K}$ has a better performance for L-PHE production than the wildtype $FruR^{WT}$ under the test conditions. Interestingly, the variant $FruR^{E173K}$ was also generated by Zhang group in an $_{L}$-PHE-producing strain HDH6-D12 by using random mutagenesis [26]. To provide more direct evidence, fed-batch fermentation was performed with the $FruR^{E173K}$ mutant and the strain PHE01.

Fed-batch fermentation of the variant $FruR^{E173K}$

To explore the performance of the best variant $FruR^{E173K}$ (PHE07) on enhancing the biosynthesis of $_{L}$-PHE, the capacity of $_{L}$-PHE production of the variant PHE07 was compared to that of the strain PHE01 by carrying out fed-batch fermentation in 50L bioreactors.

As seen in Fig. 3a, the trend of cell growth of PHE07 was significantly lower than the strain PHE01. The overall cell biomass of the strains PHE01 and PHE07 were calculated to be 41.74 ± 0.49 g/L and 37.36 ± 0.17 g/L, respectively. However, as seen in Fig. 3b, the strain PHE07 produced a significantly higher amount of $_{L}$-PHE than the reference strain PHE01 after the early stationary phase (about 20 h) until the end of the fermentation. At the end of fermentation (56 h), PHE07 produced 70.50 ± 1.02 g/L of $_{L}$-PHE, which is 23.34% higher than that of the control PHE01 (57.16 ± 1.16 g/L, Table 3). According to Table 3, PHE01 and PHE07 consumed almost the same amount of glucose. It was thus suggested that in PHE07 a part of carbon flux was redirected from the central metabolic pathway to the biosynthesis of $_{L}$-PHE. Considering the fact that FruR, as a global transcriptional regulator, mediates the flux balances among Krebs cycle, glyoxylate shunt, glycolytic pathway, gluconeogenesis pathway, and ED pathway [21], modification of the FruR protein could result in the flux being redirected toward the glyoxylate shunt and gluconeogenesis pathway, enhancing the supplying of precursors PEP and E4P for the biosynthesis of $_{L}$-PHE.

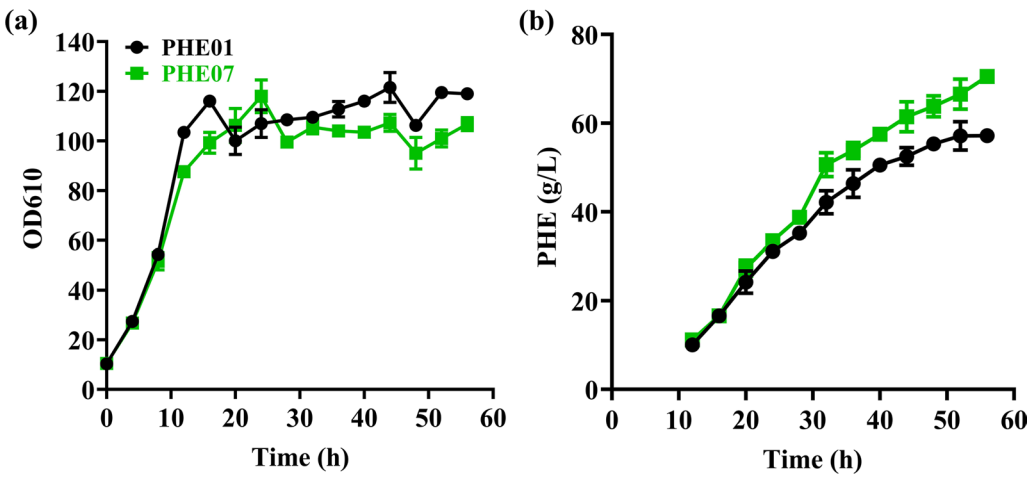

Fig. 3 Fed-batch fermentation results of the strains PHE01 (black and circle) and PHE07 (green and square). **a** Cell growth; **b** PHE production. All results are based on two independent fermentations

Table 3 Comparison of the performances of the strains PHE01 and PHE07 for $_{L}$-PHE production in fed-batch fermentation

Strains	OD_{610}	GlcC[a] (g/L)	$_{L}$-PHE (g/L)	q_{PHE} (mg/g DCW/h)	Yield (g/g)	Vp (g/L/h)
PHE01	119.25 ± 1.42	342.27 ± 10.80	57.16 ± 1.16	24.45 ± 0.02	0.167 ± 0.001	1.02 ± 0.01
PHE07	106.75 ± 0.48	340.58 ± 11.20	70.50 ± 1.02	33.69 ± 0.13	0.207 ± 0.001	1.26 ± 0.01

Fed-batch fermentations were performed in 50 L bioreactors at 37 ℃ and pH 6.8; the initial glucose concentration was 10 g/L; the initial inoculation volume ratio was 0.25. Results are given as means ± standard deviations

[a] GlcC is the calculated cumulative consumption per reactor volume

Additionally, the overall specific formation rate of $_{L}$-PHE in the strain PHE07 (33.69 ± 0.13 mg/g DCW/h, Table 3) showed an obvious advantage over that of the strain PHE01 (24.45 ± 0.02 mg/g DCW/h, Table 3). Also, it was notable that the yield of $_{L}$-PHE for PHE07 was increased to 0.207 g/g at 56 h (Table 3), whereas it was 0.167 g/g for the reference strain PHE01. These results clearly demonstrated that expressing the FruR^{E173K} protein in the strain PHE07 was able to improve the specific production rate of $_{L}$-PHE and the yield of $_{L}$-PHE significantly (by approximately 37.79% and 23.95%, respectively). The performance of PHE07 in terms of the increased $_{L}$-PHE production titer, rate, and yield makes it more attractive for industrial application. However, inconsistent with the previous reports [9, 17], overproduction of $_{L}$-PHE was realized by expression of the FruR^{E173K} protein rather than knock-out of FruR in PHE07.

As seen in the schematic diagram of the interaction between FruR and its effector fructose-1,6-bisphosphate (FBP, Additional file 3: Fig. S6), the binding cavity is surrounded by residues Asn73, Tyr76, Arg197, Ser246, Phe247, Gln291, and Arg323. According to a previous study reported by Zhu et al., [14], modification of these binding sites resulted in decrease of the binding affinity between FruR and FBP [14]. In our case, E173K mutation might also result in a low protein-effector affinity, leading to enhancement of the binding affinity between FruR and its target genes. To this end, it was thus necessary to further explore the potential regulatory mechanism for FruR^{E173K} protein in the strain PHE07 by comparative transcriptomics and metabolomics analysis.

Transcriptome and metabolome-wide effects of the regulator FruR in FruR^{E173K} in the $_{L}$-PHE producer

To assess the influence of the FruR^{E173K} protein on gene expression and the composition of intracellular metabolites in the FruR^{E173K} mutant, transcriptomics and metabolomics analysis were carried out for the FruR^{E173K} mutant (MF) as well as the wildtype PHE01 (ME). For this purpose, both strains were cultivated in the modified $_{L}$-PHE fermentation medium, and the samples were taken at the time point of 10 (Early-logarithmic phase), 20 (Mid-logarithmic phase), and 40 h (Stationary phase, Fig. 3a). In order to enable a direct comparison of the transcriptome and metabolome data, mRNA of the bacteria was isolated from the same culture samples as those used for intracellular metabolite extraction. According to the results of the metabolomics, 75 of the identified metabolites were significantly up-regulated and 98 of them significantly down-regulated (|fold change (fc)| ≤ 0.5 or ≥ 1.5; corrected $p \leq 0.05$) between the FruR^{E173K} mutant and the wildtype strain at the 20 h of cultivation (Fig. 4 and Additional file 1: Dataset S1). In parallel, transcriptomic data revealed that of 3143 profiled transcripts, 421 were significantly up-regulated and 224 significantly down-regulated in the FruR^{E173K} mutant compared to the wildtype strain, when a $|\log2fc| \geq 2.0$ and a corrected $p \leq 0.05$ in gene expression were taken as cut-off (Fig. 6 and Additional file 2: DataSet S2).

The most significant differences between the FruR^{E173K} mutant and the wildtype strain occurred in the central carbon metabolism (e.g., Krebs cycle, glyoxylate shunt, and glycolytic and gluconeogenesis pathway) and amino acid biosynthesis and metabolism (Figs. 4 and 5). The carbon flux balance between glycolytic and gluconeogenesis pathway is strictly regulated at a specific node in the EMP pathway by the regulator FruR: its effector fructose-1,6-bisphosphate (FBP) [27], meanwhile the metabolites in pentose phosphate pathway: 6-phosphogluconate (fc 261.07, p 8.88×10^{-5}) and ribose 1-phosphate (fc 1.55, p 5.67×10^{-4}), were up-regulated in the FruR^{E173K} mutant (Fig. 5a, b, Additional file 1: DataSet S1). On the transcriptome level (Fig. 6 and Additional file 2: DataSet S2), the enzymatic reactions of glycolytic and gluconeogenesis pathways were controlled correspondingly, especially the transcript levels of genes involved in the entire gluconeogenesis pathway (*gpmM*, *pfkA*, *gapA*, and *pgk*) were significantly up-regulated in the FruR^{E173K} mutant; In parallel, the transcript levels of genes associated with pentose phosphate pathway (*zwf* and *tkt*) were up-regulated (Fig. 6 and Additional file 2: DataSet S2). These results demonstrated that the modification of the regulator FruR probably activates the expression of genes involved in the gluconeogenesis pathway, which would convert the metabolic flux toward the pentose phosphate pathway and make the expression of genes associated with the pentose phosphate pathway were enhanced,

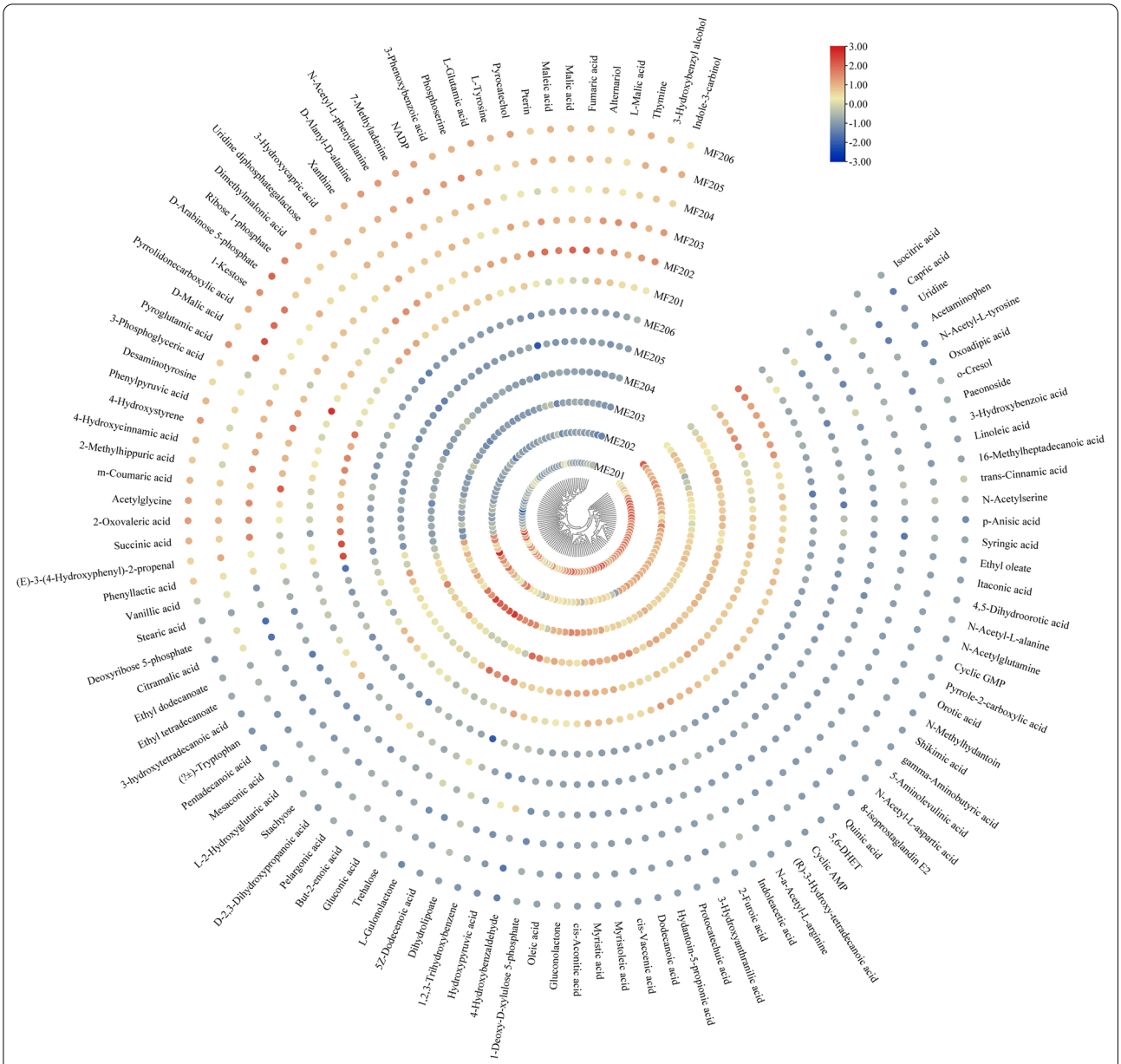

Fig. 4 Heatmap of metabolite changes for the control group ME20 and the treatment group MF20 at 20 h of cultivation. Six independent biological repetitions of each group were measured and are shown in columns. Hierarchical clustering analyses were performed on those 12 samples with known annotations. The well in red indicates metabolite is up-expressed, and the well in blue indicates metabolite is down-expressed. Source data is available for this figure at Additional file 1: DataSet S1

and eventually contributing to the accumulation of E4P, a precursor to aromatic amino acid biosynthesis. Overexpression of the genes involved in the pentose phosphate pathway, such as *zwf* and *tkt*, has been widely applied for development of aromatic amino acids (AAAs)-producing strains [11, 28, 29], while overexpression of genes involved in the gluconeogenesis pathway (*gpmM*, *pfkA*, *gapA*, and *pgk*) for enhancing the accumulation of E4P is rare reported. Thus, these targets could be potential candidates for further improvements of $_{L}$-PHE production, as well as other AAAs.

Corresponding metabolites could also be observed for the downstream Krebs cycle, where three metabolites (succinate, fumarate, and malate) were significantly up-regulated, while two metabolites (acetyl-CoA and *cis*-aconitic acid) were down-regulated in the FruR^{E173K} mutant (Fig. 5 and Additional file 1: DataSet S1). In line with this observation, parts of mRNAs of the involved

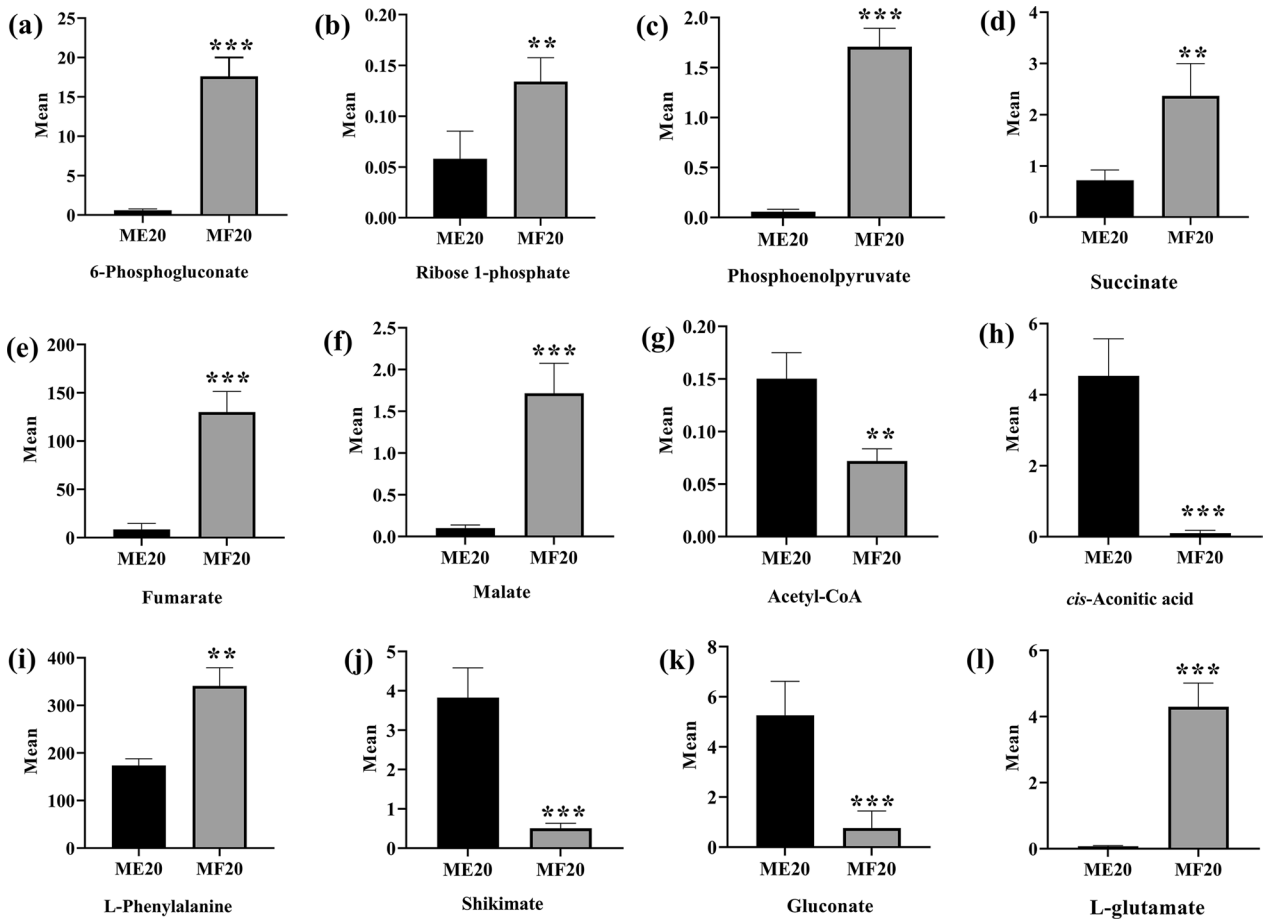

Fig. 5 Levels of intermediates involved in L-phenylalanine biosynthesis were detected in the ME20 (PHE01) and MF20 ($FruR^{E173K}$) at the cultivation of 20 h. $n = 6$ independent biological samples; $^{**}p < 0.01$, $^{***}p < 0.001$

enzymes from the Krebs cycle and glyoxylate shunt (*aceA*, *aceB*, *sucA*, and *sucD*) were activated (Fig. 6 and Additional file 2: Dataset S2), while the transcript level of genes (*aceEF*, *acnB*, and *icd*) was down-regulated in the $FruR^{E173K}$ mutant, indicating that the transcriptome data supports our metabolome data. In addition, gene *pckA* (encoding phosphoenolpyruvate carboxykinase, |log2fc| 2.75, p 1.72×10^{-21}) and gene *pps* (encoding phosphoenolpyruvate synthase, |log2fc| 3.40, p 3.45×10^{-46}) were significantly up-regulated (Fig. 6 and Additional file 2: Dataset S2), which resulted in a strong accumulation of phosphoenolpyruvate (PEP, fc 19.15, p 0.03, Fig. 5 and Additional file 1: Dataset S1), a direct precursor to aromatic amino acid biosynthesis. These results revealed that $FruR^{E173K}$ mutant activates the part of the Krebs cycle and the entire glyoxylate shunt; represses the metabolism of pyruvate and oxaloacetate and both of them are converted to PEP by enzyme Pps and PckA, respectively (Fig. 6), which resulted in the accumulation of PEP and eventually conducive to the biosynthesis of $_{L}$-PHE. PEP, as a key node between the central metabolic pathway and the AAAs biosynthetic pathway, has been converted to AAAs biosynthesis by overexpression of the genes involved in the AAAs biosynthetic pathway (such as *aroG* [9], *aroF* [7], or *aroL* [30]), and the genes related to the central metabolic pathway (e.g., *pckA* and *pps* [11, 31]), or by knockout the gene *pykF* that encodes the pyruvate kinase I [11, 32]. Moreover, as revealed in transcriptome and metabolome data in this study, overexpression of genes involved in the glyoxylate shunt (*aceA* and *aceB*) and the succinate biosynthesis (*sucA* and *sucD*), or knockout of genes *aceEF*, *acnB*, and *icd*, might also be novel strategies for development of AAAs-producing strains.

In addition to the central carbon metabolism, the $FruR^{E173K}$ mutant had a pronounced effect on the $_{L}$-PHE biosynthesis pathway. As illustrated in Figs. 4 and 5, derived from the condensation of two molecules of PEP and E4P, a 94.66-fold decrease was found for shikimate (p 3.11×10^{-5}), an intermediate of the central pathway for

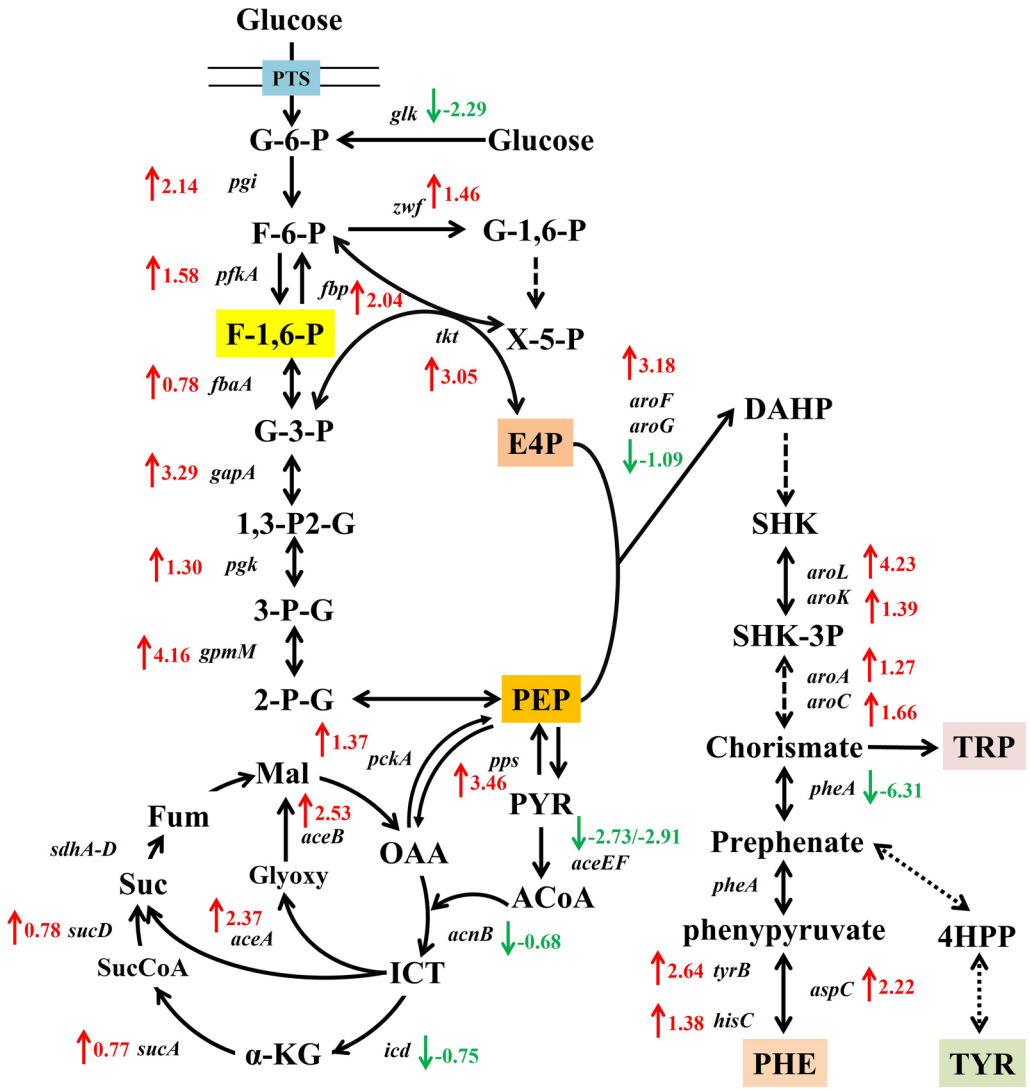

Fig. 6 Regulations of central metabolic pathway and aromatic amino acid synthesis by the catabolites repressor/activator, Cra (FruR), in *E. coli* $FruR^{E173K}$ mutant. The genes shown in aqua green boxes are under the control of FruR, some of which were identified by the experiments, and others were predicted by SELEX chip analyses or other prediction methods. The metabolite shown in a yellow box indicates the regulatory function of FruR is controlled by the intracellular concentration of the key metabolite, fructose-1,6-biphosphate. Green arrows indicate down-regulation, red arrows indicate up-regulation. Quantitative fold changes and corrected *p*-values are listed in Additional file 2: DataSet S2. Key genes for enzymes: Glucose-6-phosphate isomerase *pgi*, Fructose-1,6-bisphosphatase *fbp*, Phosphofructokinase *pfkA*, Fructose bisphosphate aldolase *fbaA*, Triose phosphate isomerase *tpi*, Glyceraldehyde 3-phosphate dehydrogenase-A *gapA*, Glyceraldehyde 3-phosphate dehydrogenase C *gapC*, Phosphoglycerate kinase *pgk*, Phosphoglycerate mutase M *gpmM*, Phosphoglycerate mutase A *gpmA*, Enolase *eno*, Pyruvate kinase I *pykF*, pyruvate kinase II *pykA*, Isocitrate lyase *aceA*, Malate synthase A*aceB*, Isocitrate dehydrogenase *icd*, 3-deoxy-D-arabino-heptulosonate-7-phosphate synthase *aroG/aroH/aroF*, 3-Dehydroquinate synthase *aroB*, 3-Dehydroquinate dehydratase *aroD*, Shikimate 5-dehydrogenase *aroE*, Shikimate dehydrogenase *ydiB*, Shikimate kinase II *aroL*, Shikimate kinase I *aroK*, 5-enolpyruvyl shikimate-3-phosphate synthase *aroA*, Chorismate synthase *aroC*, Bifunctional chorismate/prephenate dehydratase *pheA/tyrA*, Aromatic-amino-acid aminotransferase *tyrB*, Component of histidinol-phosphate aminotransferase *hisC*, Aspartate aminotransferase *aspC*

aromatic amino acids biosynthesis. This can be explained by the strong increase of the mRNA encoding the shikimate kinase AroL (|log2fc| 4.23, p 6.22×10^{-133}) and AroK (|log2fc| 1.39, p 4.26×10^{-11}), 5-enolpyruvyl shikimate-3-phosphate synthase *aroA* (|log2fc| 1.27, p 3.87×10^{-9}), and chorismate synthase *aroC* (|log2fc| 1.66, p 4.19×10^{-16}, Fig. 6 and Additional file 2: Dataset S2). Thus, it is possible that up-regulation of those genes in the $FruR^{E173K}$ mutant led to a conversion of shikimate to the AAAs biosynthesis downstream, thereby increasing

Table 4 Main strains and plasmids used in this study

Strains	Characteristics	Sources
E. coli W3110MT	W3110 derived mutant, L-tyrosine auxotrophic	Our lab
PHE01	W3110MT p15A::*pL-aroF-tyrA*$^{1-121}$*-pR-pheA*^{T326P}, kanamycin resistance	Our lab
PHE02	PHE01/pCas9, spectinomycin resistance	This work
PHE03	PHE01Δ*furR*	This work
PHE04	PHE01Δ*aroF*^{MT}*::aroF*^{WT}	This work
PHE05	PHE01Δ*pheA*^{MT}*::pheA*^{WT}	This work
PHE06	PHE01Δ*fruR::Cm*^{R}/p*mtr-RFP*	This work
PHE07	PHE01Δ*furR::furR*^{E173K}	This work
PHE08	PHE01Δ*furR::furR*^{A18P}	This work
PHE09	PHE01Δ*furR::furR*$^{L3F-L170N}$	This work
PHE10	PHE01Δ*furR::furR*$^{S75I-V160E}$	This work
PHE11	PHE01Δ*furR::furR*^{P219H}	This work
PHE12	PHE01Δ*furR::furR*^{I144T}	This work
PHE13	PHE01Δ*furR::furR*$^{E72R-P128A}$	This work
PHE14	PHE01Δ*furR::furR*^{R312G}	This work
Plasmids		
pCas	expressing Cas9 protein and offering sgRNA for removing donor plasmid, Spectinomycin resistance	[33]
pGRB	plasmid for expressing sgRNA or with offering donor DNA, Ampicillin resistance	[33]
pGRB-Δ*fruR*	pGRB *fruR*-sgRNA[a]	This work
pGRB-*aroF*^{WT}	pGRB *aroF*^{MT}-sgRNA Δ*aroF*^{MT}*::aroF*^{WT}	This work
pGRB-*pheA*^{WT}	pGRB *pheA*^{MT}-sgRNA Δ*pheA*^{MT}*::pheA*^{WT}	This work
pGRB-Δ*fruR::Cm*^{R}	pGRB *fruR*-sgRNA Δ*fruR::Cm*^{R}	This work
pGRB-*fruR*^{MT}	pGRB *Cm*^{R}-sgRNA Δ*Cm*^{R}*::fruR*^{MT}	This work
p*mtr*-RFP	pBR332 p*mtr*-RFP (L-PHE biosensor)	This work

[a] *fruR*-sgRNA, sgRNA with an N20 sequence for targeting the *fruR* gene locus

the biosynthesis of L-PHE (fc 19.15, Fig. 5). Hence, despite the central carbon metabolism, FruR^{E173K} mutant seems to also affect the AAAs pathway, especially activation of the downstream of the shikimate pathway and L-PHE pathway, which led to an accumulation of L-PHE.

As a member of the GalR-LacI family, FruR contains two functional domains: an N-terminal domain which contains a helix-turn-helix motif for DNA binding (AA 3-58 according to UniProt), and the effector binding domain located in the C terminus. FruR forms a complex with DNA in the absence of effector and acts as an activator of genes encoding gluconeogenic, Krebs cycle, and glyoxylate shunt enzymes. Upon the binding of the inducers, FruR is inactivated and the negative effect on genes encoding Entner-Doudoroff pathway and glycolytic enzymes is thus eliminated. In the previous reports on tryptophan bioproduction [17, 24], knockout of *fruR* results in function loss of the inducers and thus the genes involved in glycolysis, the Entner-Doudoroff pathway, and the PP pathway are activated and the genes involved in gluconeogenesis and the Krebs cycle are repressed. While in the case of L-PHE biosynthesis shown in this study, it was found that the changes in transcriptional levels of *fruR* gene between the FruR^{E173K} mutant (MF) and the wildtype PHE01 (ME) are not significant (Additional file 2: Dataset S2). Therefore, it is suspected that the effects of E173K mutation might be due to the decrease of the protein-effector binding affinity rather than the change of protein expression levels. As a consequence, the FruR^{E173K} mutant activates the gluconeogenesis pathway, alternative Krebs cycle, and the entire glyoxylate shunt, and no significant positive effect on the glycolysis and Entner-Doudoroff pathway was observed, as revealed by the metabolome and transcriptome analysis (Figs. 4 and 6). The different effects of FruR in the production of tryptophan and L-PHE might be due to the fact that more precursors are required for tryptophan biosynthesis. Besides the processors of PEP and E4P, PRPP and L-serine are also needed. Therefore, the balance among the pathways regulated by FruR should be modulated in different modes in order to achieve a high production. Another important reason may come from the different genetic backgrounds of the host strains, on which

the functionality of the regulatory protein is highly dependent.

Conclusion

Knockout of the *fruR* gene was first constructed in *E. coli* PHE01and the resulting strain PHE02 (PHE01Δ*fruR*) exhibited a reduced $_{L}$-PHE production, indicating that the functionality of the global regulator FruR is necessary for $_{L}$-PHE overproduction. To improve the $_{L}$-PHE production of PHE01, CRISPR/Cas9-facilitated genome-integration of the *fruR* mutagenesis libraries was coupled with the biosensor-assisted library screening approach. The best mutant strain, PHE07 (FruR^{E173K}), was obtained after several rounds of screening and characterization. Metabolomics and transcriptomics analysis suggested that the FruR^{E173K} mutant enhanced metabolic fluxes through the gluconeogenesis pathway, alternative Krebs cycle, the entire glyoxylate shunt, and the PP pathway, therefore channeling carbon fluxes to the $_{L}$-PHE biosynthetic pathway. These altered metabolic flows not only improved the utilization of carbon sources, but also enhanced the supply of precursors (PEP and E4P) for $_{L}$-PHE biosynthesis.

Methods

Strains and plasmids

The strains and plasmids used in this study are listed in Table 4. The primers used are summarized in Table S1. *E. coli* DH5α was used for plasmid construction. An $_{L}$-tyrosine auxotrophic *E. coli* PHE01 was used as the host strain for expression and $_{L}$-PHE production. To use the CRISPR/Cas9 technique for genome-editing or mutagenesis library genome-integration, the plasmid pCas9 [33] was introduced into PHE01, resulting in the strain PHE01/pCas9 (Table 4).

Implementation of CRISPR/Cas9 facilitated engineering and screening

Knocking-out of furR gene by using CRISPR/Cas9 technique

To realize the disruption of *fruR* gene, the strain PHE01/pCas9 (PHE02) was first constructed and used as the host strain. To achieve high efficiency for genome editing, the plasmid pGRB-Δ*fruR* (Additional file 3: Fig.S1) was constructed. This plasmid is able to offer the sgRNA targeting to the *fruR* gene and the homologous arms for recombination. More detailed information for the construction of pGRB-Δ*fruR* is presented in the Additional file 3.

We then followed the protocol reported by Chen and coworkers [34] to prepare the electroporation-competent cells and do the transformation. Specifically, an overnight culture (grown at 30 ℃) of the strain PHE02 was inoculated into 10 mL fresh SOC medium containing 50 μg/mL spectinomycin. After OD_{600} value reaching to 0.4–0.5, the cells were put on ice immediately for 10 min. Then, the cells were harvested by centrifugation at 4 ℃ and washed three times with precooled 10% glycerol. Competent cells were re-suspended in 400 μL precooled 10% glycerol and divided into 200 μL for each reaction. The corresponding sgRNA plasmid was mixed with the competent cells for transformation. The electroporation was done in the 0.2 cm cuvette at 2.5 kV, and the cells were suspended in 1 mL SOB medium and recovered for 2 h at 30 ℃ before plating. Plates were incubated more than 24 h at 30 ℃.

Construction of host strain for gene variant engineering and screening

To realize CRISPR/Cas9-facilitated library integration and in vivo screening, we first constructed a PHE02/p*mtr*-RFP (PHE03) strain in which an $_{L}$-PHE biosensor was expressed in the plasmid p*mtr*-RFP (Additional file 3: Fig.S3). Afterward, the native FruR enzyme of the strain PHE02 was inactivated by replacing the *fruR* gene with chloramphenicol resistance gene (*Cm^{R}*, as a selection maker), generating the strain PHE03Δ*fruR*::*Cm^{R}* (Table 4). The insertion of gene *Cm^{R}* expresses sgRNA sequence targets for further library integration using CRISPR/Cas9 technique.

Construction of gene variant library in vitro

To achieve genome-integration of mutagenesis library, it is necessary to construct a plasmid p*GRB-fruR^{MT}* (Additional file 3: Fig. S4), which contains the parts expressing the sgRNA targeting the *Cm^{R}* gene and the DNA fragment *fruR^{MT}* flanked by the corresponding homologous arms for recombination. Specifically, error-prone PCR of *fruR* gene was performed using a Diversify® PCR Random Mutagenesis Kit (PT3393-2, Takara Bio) according to the manufacturer's protocols. The purified PCR products were then ligated into the plasmid p*GRB-fruR^{MT}* using a seamless colony kit (D7010M, Beyotime). More detailed information is presented in the Additional file: 1, 2, 3.

Genome-integration and screening of fruR variant library

The *furR* variant library p*GRB-fruR^{MT}* was transferred into the competent cells of PHE03Δ*fruR*::*Cm^{R}* (containing pCas9). After incubation at 30 ℃ for more than 24 h, transformants with a stronger fluorescent signal were picked out and re-checked by streaking them on the same medium. Afterward, the candidate strains were tested by cultivation in 500 μL PHE-fermentation medium in 96-deep well plates at 30 ℃ for 24 h. Finally, the mutants giving higher medium fluorescent (MFU) and $_{L}$-PHE concentration were selected for fermentation in shake flasks. Moreover, those mutants were selected for sequencing.

Method for measurement of fluorescent intensities

The mutants containing $_{L}$-PHE biosensor with reporter RFP protein cultured in the LB medium were harvested by centrifugation and individually washed three times with the M9 medium to remove LB medium. Afterward, each mutant was inoculated with the same amount of cells into 10 mL fresh M9 medium in 50 mL conical tubes, and after cultivation of 10 h cells were subjected to fluorescence analysis using a multifunctional microplate reader. To this end, each culture was first washed three times using PBS buffer and diluted 100-fold and then RFP fluorescence was monitored using a microplate reader (Tecan M200 PRO) at an excitation wavelength of 540 nm. For fluorescent intensities, medium fluorescence unit (MFU) was calculated for each culture.

Fermentation

The fermentation medium with 1.5 g/L tyrosine was prepared as a previous report [28]. The condition for batch fermentation in shake flask was carried out in 500 mL conical flasks containing 50 mL fermentation medium inoculated with 5% (v/v) seed culture. All the batch fermentations were carried out at 37 ℃ and 250 rpm for 45 h. For fed-batch fermentation in the bioreactor, it was performed in a 50-L jar fermenter (BLBIO-10SJ-10SJ-50SJ-50SJ) with an initial broth volume of 20 L. The initial glucose concentration is 10 g/L, and it was maintained at 1–5 g/L by supplementing 700 g/L glucose in the fermentation process. Ammonia was used to maintain the pH at 6.8–7.0. The dissolved oxygen (DO) level was maintained at 25–30% saturation.

Metabolite Analysis

Sampling and LC–MS/MS analysis

Referring to the growth curve of PHE01 and PHE03 during the whole fermentation process (Fig. 3a), the samples in the time point of 10, 20, and 40 h were sampled and prepared for metabolites extraction (sextuplicate for each time point). Metabolite and transcript samples were taken simultaneously. The whole process took $\leq$5 s (metabolites) or 10 s (transcripts) per sample from sampling to flash freezing in liquid nitrogen [35]. Metabolite extraction for liquid chromatography coupled to mass spectrometry (LC–MS) analysis was performed by resuspending the cell pellet with 500 µL ice-cold acetonitrile:methanol. The cell suspension was shock-frozen again in liquid nitrogen, and 500 µL of deionized water was added. Further metabolite extraction with repeating freeze–thaw-sonification cycles followed, as described previously [36].

LC–MS/MS analyses were performed using a UHPLC system (Vanquish, Thermo Fisher Scientific) with a UPLC BEH Amide column (2.1 mm × 100 mm, 1.7 µm) coupled to QExactive HFX mass spectrometer (Orbitrap MS, Thermo). The mobile phase consisted of 25 mmol/L ammonium acetate and 25 mmol/L ammonia hydroxide in water (pH = 9.75) (A) and acetonitrile (B). The QE HFX mass spectrometer was used for its ability to acquire MS/MS spectra on information-dependent acquisition mode in the control of the acquisition software (Xcalibur, Thermo). The ESI source conditions were set as following: sheath gas flow rate as 30 Arb, Aux gas flow rate as 25 Arb, capillary temperature 350 ℃, full MS resolution as 60,000, MS/MS resolution as 7500, collision energy as 10/30/60 in NCE mode, spray Voltage as 3.6 kV (positive) or −3.2 kV (negative), respectively [37].

Data preprocessing and annotation

The raw data were converted to the mzXML format using ProteoWizard and processed with an in-house program, which was developed using R and based on XCMS, for peak detection, extraction, alignment, and integration [38, 39]. Then an in-house MS2 database (BiotreeDB) was applied in metabolite annotation. The cutoff for annotation was set at 0.3.

Transcript analysis

RNA isolation, stand-specific library preparation, and Illumina sequencing

As mentioned previously, the samples in the time point of 10, 20, and 40 h were selected and prepared for RNA isolation (triplicate for each time point). Extraction of total RNA was carried out by the Invitrogen™ TRIzol™ Reagent Kit (15596018). RNA degradation and contamination were monitored on 1% agarose gels. Total amounts and integrity of RNA were assessed using the RNA Nano 6000 Assay Kit of the Bioanalyzer 2100 system (Agilent Technologies, CA, USA). Total RNA was used as input material for the RNA sample preparations. For our samples, mRNA was purified from total RNA by using probes to remove rRNA. Strand-specific RNA-seq cDNA library preparation of the total RNA of the different samples was based on RNA adapter ligation as described previously [40]. Afterward, the quality of the library was subsequently quantified by Qubit2.0 Fluorometer, Agilent 2100 bioanalyzer, and qRT-PCR. After the library is qualified, the different libraries are pooled according to the effective concentration and the target amount of data off the machine, then being sequenced by the Illumina NovaSeq 6000. The basic principle of sequencing is to synthesize and sequence at the same time (Sequencing by Synthesis). The fluorescent images measured by the high-throughput sequencer are converted into sequence data (reads) by CASAVA base recognition. Raw data (raw

reads) of fastq format were firstly processed through in-house perl scripts [41].

Reading, mapping, bioinformatics, and statistics

Quality controlled and assessed libraries were mapped to the genome of *E. coli* strain W3110 (Acc.: chr: NC_007779) using Bowtie 2 (2.3.4.3) [42] with default parametrization. After read mapping, Rockhopper (1.2.1) was used to identify novel genes, operon, TSS, TTS, and Cis-natural antisense transcripts; RBSfinder (v1.0) [43] and TransTermH (2.0.9) [44] were used to predict SD sequence and terminator sequence, respectively; Rockhopper [45] and Blastx were used to annotate the newly predicted transgenic regions, and the unmarked transcripts were used as candidate non-coding sRNAs; RNAfold (1.8.5) [46] and IntaRNA (1.8.5) [47] were used to predict secondary structure and target gene, respectively.

The determined uniquely mapped read counts served as input to DESeq2 R package (1.20.0) [48] for pairwise detection and quantification of differential gene expression. The list of DESeq2 determined differentially expressed genes (DEGs) was filtered with a conservative cut-off: $|\log2fc| \geq 1.5$ and a corrected $p \leq 0.05$. Gene Ontology (GO) enrichment analysis of differentially expressed genes was implemented by the ClusterProfiler R package (3.8.1) with pathway information from the KEGG database (http://www.genome.jp/kegg/). Results of the comparative transcriptome analysis are given in Additional file 2: DataSet S2.

Supplementary Information

The online version contains supplementary material available at https://doi.org/10.1186/s12934-022-01954-7.

Additional file 1: DataSet 1-Differentially expressed metabolites between the FruRE173K mutant (MF) and the wildtype PHE01 (ME) at different periods of fermentation.

Additional file 2: DataSet 2-Comparisions of transcriptsome data between the FruRE173K mutant (MF) as well as the wildtype PHE01 (ME) at different periods of fermentation.

Additional file 3: Figure S1. The map of the plasmid pGRB-Δ*fruR*. This plasmid is composed of 1000 bp upstream and downstream of homologous arms for recombination and sgRNA-*fruR* sequence targeting to the *fruR* gene. **Figure S2.** The maps of the plasmids pGRB-$aroF^{WT}$ (a) and pGRB-$pheA^{WT}$ (b). **Figure S3.** The map of the PHE-biosensor p*mtr*-RFP. **Figure S4.** The map of the plasmid pGRB-$fruR^{MT}$. This plasmid is composed of 1000 bp upstream and downstream of homologous arms for recombination, sgRNA-*CmR* sequence targeting to the *CmR* gene, and donor DNA fragment $fruR^{MT}$. **Figure S5.** The map of the plasmid pGRB-Δ*fruR*::Cm^R. This plasmid is composed of 1000 bp upstream and downstream of homologous arms for recombination, sgRNA-*fruR* sequence targeting to the *fruR* gene, and donor DNA fragment *CmR*. **Figure S6.** Details of the interaction between FruR and fructose-1,6-bisphosphate. Schematic diagram of protein-ligand interaction was generated by the LIGPLOT v.4.5.3. **Table S1.** Primers used in this study.

Acknowledgements
We sincerely thank Xin Zhang from Jiaozuo Joincare Biotechnology Co. Ltd, and Qiang Luo from Livzon (Ningxia) Pharmaceutical Co. Ltd, for help with fermentation, and thank Ying Zeng from Livzon New North River Pharmaceutical Co. Ltd, for help with some of the analytics.

Author contributions
CML, LHY, HC, and ZP provided substantial contributions to the conception of the work. XZW, LYY, XGA, CQQ, and XRF substantially contributed to the acquisition, analysis, or interpretation of data. CML and LHY contributed to the manuscript drafting and revising. All authors read and approved the final manuscript.

Funding
This research was supported by National Key Research and Development Program [Grant number: 2019YFA0905404].

Availability of data and materials
Dataset that supports the findings of this study are available from the corresponding author upon reasonable request.

Declarations

Ethics approval and consent to participate
Not applicable.

Consent for publication
Not applicable.

Competing interests
The authors declare that they have no competing interests.

Author details
[1]Henan Joincare Biopharma Research Institute Co. Ltd, Jinyuan Street 8, Jiaozuo 454000, People's Republic of China. [2]Jiaozuo Joincare Biotechnology Co. Ltd, Jinyuan Street 8, Jiaozuo 454000, People's Republic of China. [3]Guangdong Provincial Key Laboratory of Research and Development and Application of Fermentation and Semi-Synthetic Drugs, Livzon New North River Pharmaceutical Co. Ltd, 1st Renmin Road, Qingyuan 511500, People's Republic of China.

Received: 9 September 2022 Accepted: 13 October 2022
Published online: 26 October 2022

References

1. Bongaerts J, Krämer M, Müller U, Raeven L, Wubbolts M. Metabolic engineering for microbial production of aromatic amino acids and derived compounds. Metab Eng. 2001;3:289–300.
2. Rodriguez A, Martnez JA, Flores N, Escalante A, Gosset G, Bolivar F. Engineering *Escherichia coli* to overproduce aromatic amino acids and derived compounds. Microb Cell Fact. 2014;13:1–15.
3. Zhang C, Zhang J, Kang Z, Du G, Chen J. Rational engineering of multiple module pathways for the production of L-phenylalanine in *Corynebacterium glutamicum*. J Ind Microbiol Biotechnol. 2015;42:787–97.
4. Ding D, Li J, Bai D, Fang H, Lin J, Zhang D. Biosensor-based monitoring of the central metabolic pathway metabolites. Biosen Bioelectron. 2020;167:112456.
5. Liu SP, Liu RX, Xiao MR, Zhang L, Ding ZY, Gu ZH, Shi GY. A systems level engineered *E. coli* capable of efficiently producing L-phenylalanine. Process Biochem. 2014;49:751–7.
6. Sprenger GA. Aromatic amino acids. In: amino acid biosynthesis~pathways, regulation and metabolic engineering. Berlin: Springer; 2006. p. 93–127.
7. Zhou H, Liao X, Wang T, Du G, Chen J. Enhanced L-phenylalanine biosynthesis by co-expression of $pheA^{fbr}$ and $aroF^{wt}$. Bioresour Technol. 2010;101:4151–6.

8. Yenyuvadee C, Kanoksinwuttipong N, Packdibamrung K. Effect of Gln151 on L-phenylalanine feedback resistance of AroG isoform of DAHP synthase in *Escherichia coli*. Sci Asia. 2021;47:40–6.
9. Chen M, Chen L, Zeng AP. CRISPR/Cas9-facilitated engineering with growth-coupled and sensor-guided in vivo screening of enzyme variants for a more efficient chorismate pathway in *E. coli*. Metab Eng Commun. 2019. https://doi.org/10.1016/j.mec.2019.e00094.
10. Minliang C, Chengwei M, Lin C, Zeng A-P. Integrated laboratory evolution and rational engineering of GalP/Glk-dependent *Escherichia coli* for higher yield and productivity of L-tryptophan biosynthesis. Metab Eng Commun. 2021;12: e00167.
11. Xiong B, Zhu Y, Tian D, Jiang S, Fan X, Ma Q, Wu H, Xie X. Flux redistribution of central carbon metabolism for efficient production of l-tryptophan in *Escherichia coli*. Biotechnol Bioeng. 2021;118:1393–404.
12. Yadav VG, De Mey M, Lim CG, Ajikumar PK, Stephanopoulos G. The future of metabolic engineering and synthetic biology: towards a systematic practice. Metab Eng. 2012;14:233–41.
13. Chong H, Geng H, Zhang H, Song H, Huang L, Jiang R. Enhancing *E. coli* isobutanol tolerance through engineering its global transcription factor cAMP receptor protein (CRP). Biotechnol Bioeng. 2014;111:700–8.
14. Zhu L-W, Xia S-T, Wei L-N, Li H-M, Yuan Z-P, Tang Y-J. Enhancing succinic acid biosynthesis in *Escherichia coli* by engineering its global transcription factor, catabolite repressor/activator (Cra). Sci Rep. 2016;6:1–11.
15. Browning DF, Busby SJ. The regulation of bacterial transcription initiation. Nat Rev Microbiol. 2004;2:57–65.
16. Berndt V, Beckstette M, Volk M, Dersch P, Brönstrup M. Metabolome and transcriptome-wide effects of the carbon storage regulator a in enteropathogenic *Escherichia coli*. Sci Rep. 2019;9:1–15.
17. Liu L, Duan X, Wu J. Modulating the direction of carbon flow in *Escherichia coli* to improve l-tryptophan production by inactivating the global regulator FruR. J Biotechnol. 2016;231:141–8.
18. Zhang F, Ouellet M, Batth TS, Adams PD, Petzold CJ, Mukhopadhyay A, Keasling JD. Enhancing fatty acid production by the expression of the regulatory transcription factor FadR. Metab Eng. 2012;14:653–60.
19. Iyer MS, Pal A, Srinivasan S, Somvanshi PR, Venkatesh K. Global transcriptional regulators fine-tune the translational and metabolic efficiency for optimal growth of *Escherichia coli*. Msystems. 2021;6:e00001-00021.
20. Ishihama A. Prokaryotic genome regulation: multifactor promoters, multitarget regulators and hierarchic networks. FEMS Microbiol Rev. 2010;34:628–45.
21. Ramseier TM, Bledig S, Michotey V, Feghali R Jr, Saier MH. The global regulatory protein FruR modulates the direction of carbon flow in *Escherichia coli*. Mol Microbiol. 1995;16:1157–69.
22. Liu L, Bilal M, Luo H, Iqbal H. Impact of transcriptional regulation by Crp, FruR, FlhD, and TyrR on L-tryptophan Biosynthesis in *Escherichia coli*. Appl Biochem Microbiol. 2021;57:319–26.
23. Cozzone AJ, El-Mansi M. Control of isocitrate dehydrogenase catalytic activity by protein phosphorylation in *Escherichia coli*. Microbial Physiol. 2005;9:132–46.
24. Sarkar D, Siddiquee KAZ, Araúzo-Bravo MJ, Oba T, Shimizu K. Effect of *cra* gene knockout together with *edd* and *iclR* genes knockout on the metabolism in *Escherichia coli*. Arch Microbiol. 2008;190:559–71.
25. Mahr R, von Boeselager RF, Wiechert J, Frunzke J. Screening of an *Escherichia coli* promoter library for a phenylalanine biosensor. Appl Microbiol Biotechnol. 2016;100:6739–53.
26. Liu Y, Zhuang Y, Ding D, Xu Y, Sun J, Zhang D. Biosensor-based evolution and elucidation of a biosynthetic pathway in *Escherichia coli*. ACS Synth Biol. 2017;6:837–48.
27. Shimada T, Yamamoto K, Ishihama A. Novel members of the Cra regulon involved in carbon metabolism in *Escherichia coli*. J Bacteriol. 2011;193:649–59.
28. Liu Y, Xu Y, Ding D, Wen J, Zhu B, Zhang D. Genetic engineering of *Escherichia coli* to improve L-phenylalanine production. BMC Biotechnol. 2018;18:1–12.
29. Yakandawala N, Romeo T, Friesen AD, Madhyastha S. Metabolic engineering of *Escherichia coli* to enhance phenylalanine production. Appl Microbiol Biotechnol. 2008;78:283–91.
30. Ding D, Liu Y, Xu Y, Zheng P, Li H, Zhang D, Sun J. Improving the production of L-phenylalanine by identifying key enzymes through multi-enzyme reaction system in vitro. Sci Rep. 2016;6:32208.
31. Shen T, Liu Q, Xie X, Xu Q, Chen N. Improved production of tryptophan in genetically engineered *Escherichia coli* with TktA and PpsA overexpression. J Biomed Biotechnol. 2012;2012: 605219.
32. Siddiquee KA, Arauzo-Bravo MJ, Shimizu K. Effect of a pyruvate kinase (*pykF*-gene) knockout mutation on the control of gene expression and metabolic fluxes in *Escherichia coli*. FEMS Microbiol Lett. 2004;235:25–33.
33. Jiang Y, Chen B, Duan C, Sun B, Yang J, Yang S. Multigene editing in the *Escherichia coli* genome via the CRISPR-Cas9 system. Appl Environ Microbiol. 2015;81:2506–14.
34. Chen L, Zeng A-P. Rational design and metabolic analysis of *Escherichia coli* for effective production of L-tryptophan at high concentration. Appl Microbiol Biotechnol. 2017;101:559–68.
35. Bolten CJ, Kiefer P, Letisse F, Portais J-C, Wittmann C. Sampling for metabolome analysis of microorganisms. Anal Chem. 2007;79:3843–9.
36. Yanes O, Tautenhahn R, Patti GJ, Siuzdak G. Expanding coverage of the metabolome for global metabolite profiling. Anal Chem. 2011;83:2152–61.
37. Dunn WB, Broadhurst D, Begley P, Zelena E, Francis-McIntyre S, Anderson N, Brown M, Knowles JD, Halsall A, Haselden JN. Procedures for large-scale metabolic profiling of serum and plasma using gas chromatography and liquid chromatography coupled to mass spectrometry. Nat Protoc. 2011;6:1060–83.
38. Cai Y, Weng K, Guo Y, Peng J, Zhu Z-J. An integrated targeted metabolomic platform for high-throughput metabolite profiling and automated data processing. Metabolomics. 2015;11:1575–86.
39. Smith CA, Want EJ, O'Maille G, Abagyan R, Siuzdak G. XCMS: processing mass spectrometry data for metabolite profiling using nonlinear peak alignment, matching, and identification. Anal Chem. 2006;78:779–87.
40. Nuss AM, Heroven AK, Waldmann B, Reinkensmeier J, Jarek M, Beckstette M, Dersch P. Transcriptomic profiling of Yersinia pseudotuberculosis reveals reprogramming of the Crp regulon by temperature and uncovers Crp as a master regulator of small RNAs. PLoS Genet. 2015;11:e1005087.
41. Cock PJ, Fields CJ, Goto N, Heuer ML, Rice PM. The Sanger FASTQ file format for sequences with quality scores, and the Solexa/Illumina FASTQ variants. Nucleic Acids Res. 2010;38:1767–71.
42. Langmead B, Salzberg SL. Fast gapped-read alignment with Bowtie 2. Nat Methods. 2012;9:357–9.
43. Suzek BE, Ermolaeva MD, Schreiber M, Salzberg SL. A probabilistic method for identifying start codons in bacterial genomes. Bioinformatics. 2001;17:1123–30.
44. Kingsford CL, Ayanbule K, Salzberg SL. Rapid, accurate, computational discovery of Rho-independent transcription terminators illuminates their relationship to DNA uptake. Genome Biol. 2007;8:1–12.
45. McClure R, Balasubramanian D, Sun Y, Bobrovskyy M, Sumby P, Genco CA, Vanderpool CK, Tjaden B. Computational analysis of bacterial RNA-Seq data. Nucleic Acids Res. 2013;41:e140–e140.
46. Hofacker IL, Stadler PF. Memory efficient folding algorithms for circular RNA secondary structures. Bioinformatics. 2006;22:1172–6.
47. Busch A, Richter AS, Backofen R. IntaRNA: efficient prediction of bacterial sRNA targets incorporating target site accessibility and seed regions. Bioinformatics. 2008;24:2849–56.
48. Anders S, Huber W. Differential expression analysis for sequence count data. Nat Precedings. 2010. https://doi.org/10.1038/npre.2010.4282.1.

Publisher's Note